Monthly Notices
of the
ROYAL ASTRONOMICAL SOCIETY

MNRAS **497,** 2501–2516 (2020)
Advance Access publication 2020 July 20

doi:10.1093/mnras/staa2113

Restoring the night sky darkness at Observatorio del Teide: First application of the model Illumina version 2

Martin Aubé,[1,2,3]★ Alexandre Simoneau,[3] Casiana Muñoz-Tuñón,[4,5] Javier Díaz-Castro[4,5] and Miquel Serra-Ricart[4,5]

[1]*Département de physique, Cégep de Sherbrooke, Sherbrooke, 475 rue du Cégep, Sherbrooke, Québec J1E 4K1, Canada*
[2]*Department of Physics, Bishops University, 2600 College St, Sherbrooke, Québec J1M 1Z7, Canada*
[3]*Département de géomatique appliquée, Université de Sherbrooke, 2500 Boulevard de l'Université, Sherbrooke, Québec J1K 2R1, Canada*
[4]*Instituto de Astrofísica de Canarias, Calle Vía Láctea, s/n, 38205 San Cristóbal de La Laguna, Santa Cruz de Tenerife 38205, Spain*
[5]*Departamento de Astrofísica, Universidad de La Laguna (ULL), 38205 La Laguna, Tenerife, Spain*

Accepted 2020 July 13. Received 2020 July 13; in original form 2020 May 27

ABSTRACT

The propagation of artificial light into real environments is complex. To perform its numerical modelling with accuracy, one must consider hyperspectral properties of the lighting devices and their geographic positions, the hyperspectral properties of the ground reflectance, the size and distribution of small-scale obstacles, the blocking effect of topography, the lamps angular photometry and the atmospheric transfer function (aerosols and molecules). A detailed radiative transfer model can be used to evaluate how a particular change in the lighting infrastructure may affect the sky radiance. In this paper, we use the new version (v2) of the Illumina model to evaluate a night sky restoration plan for the Teide Observatory located on the island of Tenerife, Spain. In the past decades, the sky darkness was severely degraded by growing light pollution on the Tenerife Island. In this work, we use the contribution maps giving the effect of each pixel of the territory to the artificial sky radiance. We exploit the hyperspectral capabilities of Illumina v2 and show how the contribution maps can be integrated over regions or municipalities according to the Johnson–Cousins photometric bands spectral sensitivities. The sky brightness reductions per municipality after a complete shutdown and a conversion to light-emitting diodes are calculated in the Johnson–Cousins *B, V, R* bands. We found that the conversion of the lighting infrastructure of Tenerife with LED (1800 and 2700 K), according to the conversion strategy in force, would result in a zenith *V*-band sky brightness reduction of $\approx$0.3 mag arcsec^{-2}.

Key words: atmospheric effects – methods: numerical – methods: observational – site testing – software: data analysis – software: simulations.

1 INTRODUCTION

The propagation of light in the nocturnal environment involves multiple physical interactions (Aubé 2015). To model that propagation with reasonable level of accuracy, one must include the information about the optical properties of the artificial light sources (spectral power distribution, angular emission) and their positions (latitude, longitude, elevation, and height above ground). Other parameters such as the presence of blocking obstacles such as trees and buildings, the spectral ground reflectance and the optical transfer function of the atmosphere (including aerosols) significantly influence light propagation (Aubé 2007; Patat 2008; Falchi 2011; Pun & So 2012; Aubé et al. 2014; Pun et al. 2014; Puschnig, Posch & Uttenthaler 2014; Kyba et al. 2015; Sánchez de Miguel 2015; Sánchez de Miguel et al. 2017).

The use of numerical models to study light pollution dates back to the 1980s with the Garstang model (Garstang 1986). Numerical models allow a full control of the environmental parameters and provide the possibility to identify the origin of the light detected at a particular location in any viewing angle. The Garstang model contained many simplifying assumptions, mainly motivated by the low power of computers available at that time. Since then, many models have been developed with increased complexity to better describe the light pollution propagation in the nocturnal environment (Aubé et al. 2005; Aubé 2007; Baddiley 2007; Kocifaj 2007; Luginbuhl et al. 2009; Luginbuhl et al. 2009; Cinzano & Falchi 2013; Aubé 2015; Falchi et al. 2016; Aubé & Simoneau 2018).

The Teide Observatory or Observatorio del Teide (OT) was founded in 1964. It is located in the Canary island of Tenerife at 2390 m of altitude. It is operated by the Instituto de Astrofísica de Canarias (IAC). It hosts many international telescopes and is the reference in solar astronomy. It benefits from good seeing conditions and good image quality (Vernin & Muñoz-Tuñón 1992; Vernin & Munoz-Tunon 1994; Munoz-Tunón, Vernin & Varela 1997; Munoz-Tunón 2002; Vernin et al. 2011; Pérez-Jordán et al. 2015). Its artificial skyglow increased with the development of the touristic industry and with the general population increase. Its research capacities in the visible have been considerably reduced accordingly. For that reason, subsequent major optical telescopes were built at Roque

★ E-mail: martin.aube@cegepsherbrooke.qc.ca

de los Muchachos Observatory (ORM) on the nearby island of La Palma. To protect ORM sky from being altered too by light pollution, la 'ley del cielo' (Juan Carlos I 1988; Gómez 1992; de Santamaría Antón 2017), a national light pollution abatement, was voted by the Spanish government. This law comprises strict regulations to the lighting practices on the Island of La Palma but also some important restrictions for the Island of Tenerife. In 1997, the Spanish Government has subsidized the cost of a programme of street lighting replacement on La Palma island to minimize light pollution (Díaz-Castro 1998). The areas of Tenerife island facing ORM, hereafter called the protected area, experience more restrictive lighting rules than the rest of the island (hereafter called unprotected area). Because of that law, in the protected area, any lighting replacement has to be done using phosphor-converted amber light (PCamber) light-emitting diodes (LED) with a reduction of output flux of 20 per cent (i.e. output flux is 0.8 of initial value). In the unprotected area, lighting replacement has to be done using 2700 Kelvin LEDs (LED2700K) with an output flux reduction of 70 per cent (i.e. output flux is 0.3 of its initial value). The smaller flux reduction for the protected area is explained by the fact that for this area, in the past, the allowed output flux was more restrictive than in the unprotected area. Basically, the protected area luminous flux was already reduced. At the end, when all light fixtures of the island will be converted to LEDs, both areas will have similar lighting levels. For the whole island of Tenerife, there is an additional flux reduction after midnight (output flux after midnight is 0.65 of the output flux before midnight).

The aim of this paper is to show up to what extent darkness of the sky around zenith at OT can be improved on the basis of its artificial sky radiance reduction. To achieve that, we first model the multispectral artificial sky radiance towards zenith and at 30° from zenith for the present situation. The crucial step to reach this first milestone was to define the lighting infrastructure and the obstacles properties all over the modelling domain. The modelled present artificial radiance is compared with all-sky transmission monitor (ASTMON; Aceituno et al. 2011) sky brightness (SB) measurements in the *B*, *V*, and *R* Johnson–Cousins (JC) photometric bands for instruments installed at OT and ORM. Such a comparison is required to get a relevant estimate of the natural SB. This natural component comes from many sources such as the starlight, the sky glow, the zodiacal light, and so on. The natural SB and corresponding natural radiance are used to transform the calculation of the artificial sky radiance into the total SB (artificial + natural). In addition to modelling the present situation, two other modelled scenarios were performed to determine the effect of a full replacement of the light fixtures by: 1- PCamber, and 2- LED2700K. For these last two scenarios, we maintained the output flux equal to its present values. The results are weighted by the output flux reduction rules identified for the protected and unprotected areas.

2 METHODOLOGY

A simulation of the OT and ORM skies have been done by Aubé & Kocifaj (2012) using version 0 of Illumina (v0). It was a comparison experiment with the MSNsRAu model (Kocifaj 2007). Among many differences with the version 2 (v2) used in this paper, Illumina v0 was monochromatic and was using the Defense Meteorological Satellite Program – Operational Linescan System (DMSP-OLS; Imhoff et al. 1997; Elvidge et al. 1999) satellite data with much lower resolution and bad radiometric accuracy compared to Visible Infrared Imaging Radiometer Suite Day Night Band (VIIRS-DNB; Elvidge et al. 2017) used in v2. It also had a crude correction for subgrid obstacles.

There are not many methods to evaluate to what extent the sky quality of OT can be improved on the basis of its artificial sky radiance reduction. One of them can be that proposed by Bara & Lima (2018) where they compute the relative contribution of an area to the SB of another. The present method is similar in the sense that we also integrate the contribution over municipalities, but since we are only concerned about a precise observing location we can model exactly the contributions to the sky radiance of the location using a complete radiative transfer model such as Illumina instead of relying on the use of uniform point-spread functions. In this paper, we are using the new version (v2) of the radiative transfer model Illumina to simulate the sky radiance in several wavelengths (spectral bins). Prior to the numerical calculations, it is important to define, as accurately as possible, the light fixture inventory, a list of the properties of the light sources (spectral power distribution and angular emission functions) and obstacles of the domain. This is probably the most difficult part of the work. Illumina do not requires a global angular emission function but only the lamps emission functions. This parameter is defined per pixel according to the mix of lamp models encountered in that pixel. The reflected light component of the global emission is calculated according to the Lambertian reflectance law but is managed by the model as a different light path because that the obstacles blocking effect do not affect equally the light from the fixture and the light from ground reflection. Most of the time the lamps angular emissions are not precisely known and to compensate this lack of information, we are working with a local expert who help us to define the typical mix of lamps inside a set of circular zones. As a result of the numerical calculations, we can exploit the modelled sky radiance in every spectral bin and combine them to create the artificial sky spectrum. We can also exploit the contribution maps. Such maps give the geographical distribution of the origin of the modelled sky radiance. There is one contribution map per spectral bin, per viewing angle, and per lighting scenario. We integrated the contribution maps using the three JC bands (*B*, *V*, *R*) to compare them to the observed SB. The natural radiance in each JC band needs to be determined to calculate the total SB and radiance (natural + artificial). Contribution maps are also integrated over geographical limits of Tenerife municipalities and over the protected/unprotected area of the Tenerife Island. Such method is also applied to lighting conversion plans which allow the evaluation of the expected radiance reductions and SB decrease associated with the conversion or shutdown of each municipality or area.

2.1 Illumina v2 model

Illumina is a heterogeneous radiative transfer model dedicated to the simulation of the artificial sky radiance in any wavelength (Aubé et al. 2005; Aubé 2007; Aubé 2015; Aubé & Simoneau 2018). The model is calculating the following physical interactions: (1) the aerosol (scattering and absorption) and molecular extinction (scattering only), (2) the first and second order of scattering, (3) the ground reflection (lambertian), (4) the lamp flux, (5) the lamp angular emission function (horizontally averaged), (6) the topography, (7) the subgrid obstacles blocking (trees and buildings when the horizontal and vertical resolution cannot resolve them), and (8) the reflection by overhead clouds. Illumina cannot yet calculate the molecular absorption. For that reason, the use of Illumina must be restricted to the atmospheric windows but especially to the visible range. Since we used the newly released version of the model, it is worth highlighting the changes compared to the previous version (v1). The basic novelties of the model comprise

(i) An improvement of the calculation of the scattering probability and extinction. The probability of scattering is obtained from

$$p = 1 - \exp\left(\frac{\ln(T_\infty)\exp(-z/H)d}{H}\right), \quad (1)$$

where p multiplied by the flux intercepted by the scattering voxel and multiplied again by the scattering phase function (sr^{-1}; aerosols or molecules) for a given scattering angle gives the radiant intensity (Wsr^{-1}) at that scattering angle. T_∞ is the vertical transmittance of the aerosols or molecules for the entire atmospheric vertical column. H is the scale height ($H = 8$ km for molecules and 2 km for aerosols), z is the altitude above ground, and d is the length of the scattering voxel (1 m in Illumina v2). Similarly, the transmittance of a light path is given by equations (2) and (3) for a horizontal and an oblique light beam, respectively:

$$T = \exp\left(\frac{\ln(T_\infty)\exp(-z/H)d}{H}\right), \quad (2)$$

$$T = \exp\left(\frac{\ln(T_\infty)}{\cos(\theta_z)}\left[e^{-z_a/H} - e^{-z_b/H}\right]\right), \quad (3)$$

where d is the horizontal distance of the light path, z_a and z_b are the bottom and top heights, and θ_z is the zenith angle. T_∞ for molecules ($T_{m\infty}$) is obtained using the extinction coefficient given by Kneizys et al. (1980) in their equation 18 (see equation 5 next). For aerosols, $T_{a\infty}$ is given by equation (6).

(ii) The improvement of the accuracy in determining the solid angles. Especially when the scattering medium is located near the source, the first-order scattering point, or the observer. In v1, the 3D space was divided into a fixed and coarse mesh grid, while in v2, we are defining small voxels on the fly. No vertical mesh grid is used anymore. The removal of the vertical mesh reduced greatly the memory requirements to run the model and also removed digital artifacts coming from the evaluation of the solid angle of a rectangular prism as seen from different angles.

(iii) The cloud base height can be set by the user, and a correction for the cloud fraction was added on the basis of Ścieżor (2020) observations. We do not use this feature in this work since we are only concerned about clear skies.

(iv) The addition of the direct radiance calculation. In v1, only the sky radiance was calculated. No direct sight to the light fixtures was allowed. This feature is not used in this work since we are focusing on the sky radiance. The direct radiance data are more suited for health and ecosystem studies.

(v) The Moderate Resolution Imaging Spectroradiometer (MODIS) reflectance product used in v1 is replaced by a weighted combination of surface reflectances to be defined by the user. This change has been implemented because (1) the low resolution of the MODIS data (500 m) that include many types of surface at the street-level scale so that the reflectance was not only representative of the ground below the light fixtures but rather of an average of surfaces, some lighted, some not; (2) the coarse resolution of VIIRS-DNB of 750 m do not allow the precise localization of the source and this is not enough accurate to identify the right reflectance to use even if we use high-resolution reflectance data such as the one from the Land Satellite (Masek et al. 2006); 3- satellite-based evaluation of the reflectance can be biased by obstacles that can hide the lighted surfaces and then introduce significant mismatch between the detected reflectance and the one of the surfaces underlying the lamp fixture. In v2, the reflectance is constant for all the modelling domain but has to be representative of the ground underlying the lighting devices. The ASTER spectral library (Baldridge et al. 2009) is routinely used for that purpose.

(vi) The introduction of a multiscale grid that can allow a finer description of the environment near the observer. With this new feature, there is virtually no limit to the spatial resolution. In v1, the spatial resolution was fixed to 1 km. With v2, one can use very high resolution lidar data and then resolve the 3D buildings and trees effect on the light propagation. In v1, only a subgrid statistical obstacle correction was possible. Note that such statistical subgrid correction is still available in v2, depending on the resolution used in the multiscale definition of the modelling domain.

(vii) The point source inventory can be directly used in the model to improve satellite-derived inventory. In v1, only satellite-derived inventory was possible. We do not use this feature in this work.

As for Illumina v1, Illumina v2 requires an 'as accurate as possible' definition of a set of input data:

(i) angular emission function of the lamps*;
(ii) spectra of the lamps*;
(iii) lamp flux;
(iv) lamp height relative to the ground;
(v) obstacles properties (height, distance, filling factor)*;
(vi) underlying ground spectral reflectance;
(vii) topography;
(viii) minimum ground surface atmospheric pressure;
(ix) relative humidity;
(x) τ_a, Angström coefficient (α) and the aerosol model

Most of them are currently quite easy to define except the ones marked with an asterisk. Their determination requires the collaboration with a local expert that has good knowledge of the lighting infrastructure. We hope that with the rapid evolution of remote sensing techniques, having a local expert will not be required in a near future.

2.2 Modelling experiments

The aim of that work is to the evaluate the current level of light pollution and its possible change upon conversion of the lighting infrastructure with less-polluting devices and better lighting practices. In that scope, it is very important to correctly define the geographical domain, the lighting infrastructure, and environmental properties over that domain. To accurately model the contribution of the different municipalities of Tenerife Island on the sky radiance at OT, we defined a finer resolution inventory for Tenerife while keeping a coarse definition for the other islands. It is well known, and since a long time, that the effect of light pollution is decreasing rapidly with distance (Bertiau et al. 1973; Treanor 1973; Berry 1976). This fact stresses the importance of a better definition of the sources close to the observer. The experiment use 14 layers ranging from 20 m of resolution in the first central layer to a resolution of ≈1493 m for the 14th layer. The resolution scale factor between two consecutive layers is 1.393. This number was chosen to reduce the computing time while keeping a satisfactory accuracy of the calculations. Given that, the resolution of the second layer is ≈28 m, the third ≈39 m and so on. The dimensions of each layer were 255 × 255 pixels.

Figs 1 and 2 show the various circular zones that were defined to characterize the different lighting and environment properties. On a given circular zone, we assume that the statistics of the lamp parameters (percentage of each spectrum, of each angular emission functions, and of each lamp height) and the obstacles properties are uniform. This subdivision in circular zones aim to render it possible to build the inventory with the local expert. But in practice, it is often true that lighting practices vary per sectors of a territory. This is

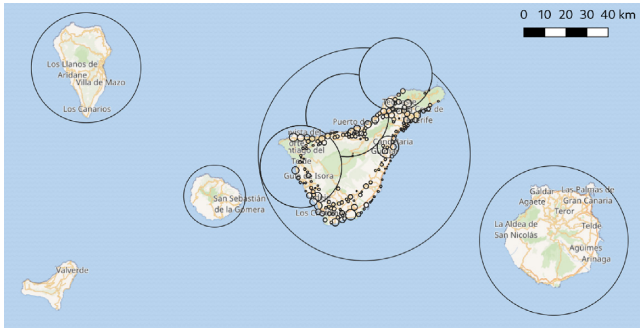

Figure 1. Circular zones used to define the properties of lighting devices and of the obstacles over the whole modelling domain. In the setting of the properties, the smaller zones overwrite the larger if ever there is an intersection between them.

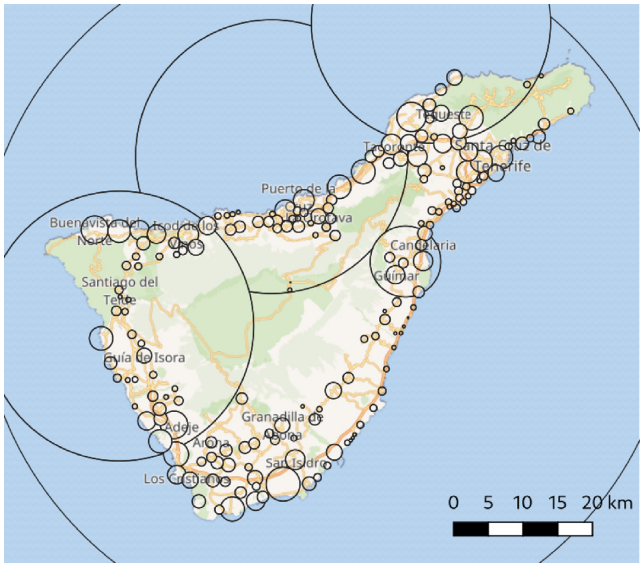

Figure 2. Enlargement of Fig. 1 showing circular zones used to define the properties of lighting devices and of the obstacles over the Tenerife Island.

relying mostly on different use of the territory (industrial, residential, etc.) but also on historical reasons. The light flux inside a given zone can vary given that it is derived using the VIIRS-DNB satellite monthly data (2019 April in this study). April data was the most recent monthly composite available. Topography also varies inside a zone. The method used to convert VIIRS-DNB into flux is explained in Aubé & Simoneau (2018). The complete set of data used for the inventory is given in Table A1.

The modelling domain can be seen in Fig. 3. This figure corresponds to the original VIIRS-DNB upward radiance data. The overall modelling domain covers ≈380 km E-W by ≈380 km N–S. The domain is centred on the observer position at OT (28.301197° N, 16.510761° W). We assume the observer to be 5 m above ground to simulate a telescope.

A zoomed view on Tenerife Island is provided on Fig. 4. In Fig. 4, we filtered the original VIIRS-DNB radiances with a threshold of 0.8 nW sr^{-1} cm^{-2}. Such a threshold allowed to remove the background light over the ocean surface along with over the unlighted dense forest of the islands.

The calculations are made for 14 25 nm-wide spectral bins covering the spectral range of 380–730 nm. The sea-level air pressure is set to 101.3 kPa with an air relative humidity of 70 per cent. The

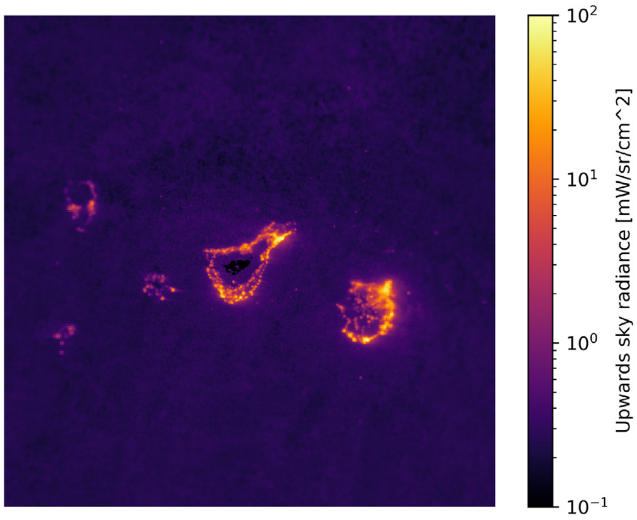

Figure 3. Original VIIRS-DNB radiances over the modelling domain.

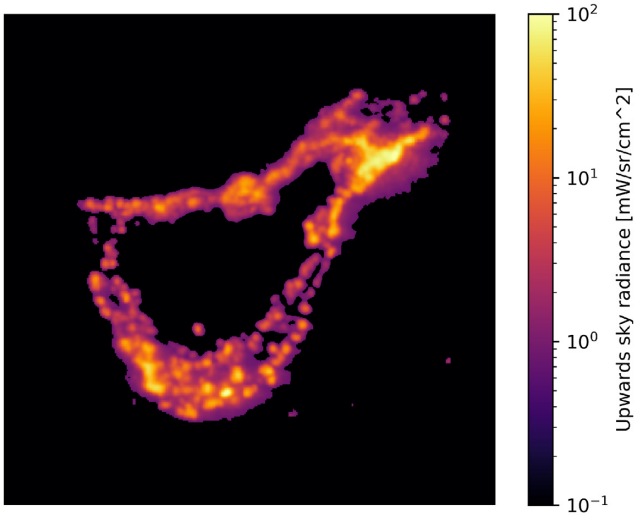

Figure 4. Filtered VIIRS-DNB data over the Tenerife Island.

relative humidity if used to modify the scattering and absorption cross sections and phase functions of aerosols. The sky is defined as cloudless. The maximum distance to calculate the effect of reflection on the ground is set to 9.99 m and the ground reflectance is defined by a weighted spectrum obtained assuming 90 per cent of asphalt and 10 per cent of grass. Reflectance spectra are taken from the ASTER spectral library (Baldridge et al. 2009). We are using a τ_a at 500 nm of 0.04 and an angstrom coefficient of 1.1. Both values corresponding to the average of clear sky conditions for that period (2019 April) according to the Izaña sunphotometer of the Aerosol Robotic Network (Holben et al. 1998). This Izaña sunphotometer is located only about 1 km away from OT and is at almost the same altitude. We used the maritime aerosol model as defined by Shettle & Fenn (1979).

We modelled three cases: (1) the present situation, (2) a complete conversion of the lamps to LED2700K, and (3) a complete conversion to PCamber. For both conversion scenarios, we first assumed that the output luminous flux was kept identical as it is in the present situation. At the end, to estimate the effect of real conversions, we weigh these results by their output luminous flux reductions according to the

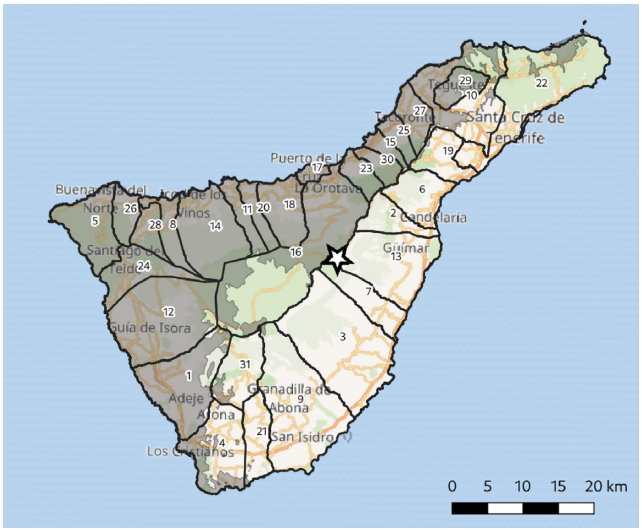

Figure 5. Limits of the various municipalities of Tenerife and protected (grey)/unprotected area. The observatory is marked by a star. The green colour represent natural parks and reserves.

legal prescriptions described in the introduction (−20 per cent in the protected area and −70 per cent in the unprotected). In addition, we assume that replacement in the protected area is done using PCamber while LED2700K to be used in the unprotected area.

2.3 Integration over geographical limits and JC bands

There is one artificial radiance contribution map for each viewing angle and spectral bin. Since we are focused on the analysis of the SB in the *JC* bands (*B*, *V*, *R*), we need to integrate the spectral information over each band. The process consists of doing the product of the spectral sensitivity of the JC band integrated over the spectral bin by the artificial radiance of that bin and integrate this quantity over the spectral range for each pixel of the modelling domain. The result is the JC band artificial radiance contribution map. Knowing the geographical limits of the municipalities and protected/unprotected areas, it is then possible to add up radiances of all pixel falling inside the limits of each municipality or area. Again, we obtain an artificial radiance but it corresponds to the artificial radiance in JC bands for each municipality or area. The limits of the various municipalities and areas of Tenerife Island are illustrated in Fig. 5. The star on that figure illustrates the position of the OT.

2.4 Atmospheric and obstacle correction to the VIIRS-DNB inversion

At the moment of writing this paper, Illumina do not correct for the VIIRS-DNB signal reduction caused by the atmospheric extinction and obstacles blocking. These corrections will soon be incorporated into the model. Their effect on each pixel of the modelling domain should be different because the obstacles and angular emission of light vary from one pixel to the other. In this study, we have made an approximate correction on the modelling output results instead of the modelling inputs. For the atmospheric correction, the correction is the same everywhere.

To compensate for the molecular transmittance (T_m) and the aerosol transmittance (T_a), we use the following expression:

$$F_T = \frac{1}{T_{\mathrm{a}\infty} T_{\mathrm{m}\infty}}. \tag{4}$$

Table 1. Percentile 75 ASTMON sky brightness measurements and differences in 2019 April at OT and ORM. The Δ_S values of that table are used to determine precisely the correction factor F_o.

Band	Product	S (OT) (mag arcsec^{-2})	S (ORM) (mag arcsec^{-2})	Δ_S (mag arcsec^{-2})
B	P75	22.11	22.26	0.15
V	P75	21.06	21.52	0.46
R	P75	20.79	20.83	0.04

Table 2. Percentile 99 ASTMON sky brightness measurements for 2018–2019 at ORM.

Band	Product	*S* (ORM) (mag arcsec^{-2})	Error (mag arcsec^{-2})	nb data –
B	P99	22.66	0.03	814
V	P99	21.84	0.02	762
R	P99	21.18	0.01	1,157

The molecular transmittance is calculated with equation (5) derived from Kneizys et al. (1980).

$$T_{\mathrm{m}\infty} = \exp\left(\frac{-1}{\lambda^4\left(115.6406 - \frac{1.335}{\lambda^2}\right)}\right), \tag{5}$$

where λ is in units of μm. The aerosol transmittance is calculated using

$$T_{\mathrm{a}\infty} = e^{-\tau_\mathrm{a}}, \tag{6}$$

where τ_a is calculated at any wavelength ($\tau_\mathrm{a}(\lambda)$) from τ_a at 500 nm ($\tau_\mathrm{a}(0.5\ \mu\mathrm{m})$) and with the Angstrom exponent α.

$$\tau_\mathrm{a}(\lambda) = \tau_\mathrm{a}(0.5\mu\mathrm{m})\left(\frac{\lambda}{0.5}\right)^{-\alpha}. \tag{7}$$

F_T can be easily estimated for the effective wavelength (λ_e) of the *B*, *V*, and *R* bands given in Table 4.

The buildings and trees are unresolved obstacles in the model, but we include their statistical effects. However, they are only considered to solve the radiative transfer but not to produce the input data. Obstacles blocking is determined by the average horizontal distance between the lamp and the obstacle (d_o), the average lamp height (h_l), and the average obstacle height (h_o) along with the obstacle filling factor (f_o). f_o accounts for the fact that not all the light is intercepted by the obstacles, a part of it can pass through because there can be some space between the buildings and trees. These parameters were defined while building the inventory (see Table A1). In Table A1, 'Obst. Distance' is equal to $2 \times d_o$. The VIIRS-DNB radiance monthly product is an average of radiances corresponding to a variety of zenith angles from 0 to 70°. But many of these angles are partly blocked by the subgrid obstacles. This blocking effect impacts in different ways the VIIRS-DNB radiance monthly product. There could be two components to the upward radiance: (1) the direct light and (2) the light reflected by the ground and obstacles surfaces. In most cases, the second component is the dominant one. This is because most light fixtures do not emit significantly at $\theta_z < 70°$. Light coming from windows and sports facilities are of course emitting part of their light at that range of angles but since our study is for after midnight situation and that we used after midnight satellite data, we assume that their contributions were small at that time compared to other sources. If we define the obstacle correction factor as F_o, we can write the corrected radiance R_a as a function of the uncorrected artificial radiance ($R_\mathrm{a}{}^*$) as follows:

Table 3. Correction factors to the modelled radiance assuming $h_o = 9, f_o = 0.9$, and $d_o = 6$.

Band	λ_e (nm)	T_m –	T_a –	F_T –	F_o –
B	436.1	0.775	0.922	1.40	4.6
V	544.8	0.903	0.938	1.18	4.6
R	640.7	0.949	0.948	1.11	4.6

Table 4. Zero-point radiances for the JC photometric system derived from Bessell (1979).

Band	λ_e nm	FWHM nm	R_0 W m^{-2} sr^{-1}
B	436.1	89	254.3
V	544.8	84	131.4
R	640.7	158	151.2

Table 5. Natural sky brightness, background radiances, artificial radiances, and total radiances towards zenith at OT in the *B, V, R* bands. *B* and *V* were determined using Benn & Ellison (1998), while *R* was determined with P99 measurements of table 2.

Band	S_{bg} (mag arcsec^{-2})	R_{bg} (Wm^{-2}sr^{-1})	R_a (Wm^{-2}sr^{-1})	R (Wm^{-2}sr^{-1})
B	22.73	2.06E-07	3.89E-08	2.45E-07
V	21.93	2.22E-07	2.20E-07	4.42E-07
R	21.18	5.10E-07	2.24E-07	7.34E-07

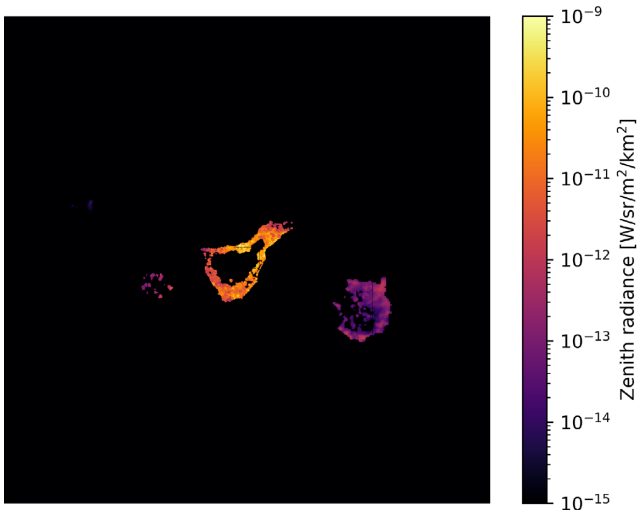

Figure 6. Contribution of the different part of the Canary Islands to the *V*-band artificial zenith sky radiance at OT.

$$R_a \approx R_a^* F_T F_o. \tag{8}$$

If we assume that the street surface is the most lighted surface and then neglect the reflected light from the obstacles walls, we can define the limit zenith angle that allows reflected light to reach the satellite. This angle is given by

$$\theta_{lim} = \arctan\left(\frac{d_o}{h_o}\right). \tag{9}$$

The obstacles correction factor can be calculated by a weighting function of the solid angles.

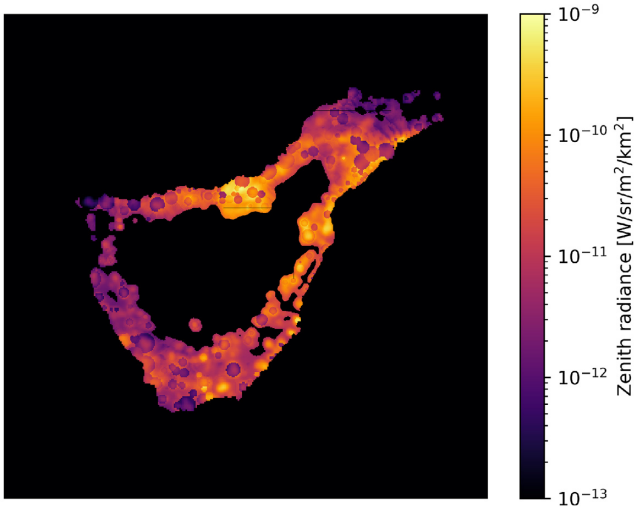

Figure 7. Contribution of the different part of the Tenerife Island to the *V*-band artificial zenith sky radiance at OT.

$$F_o \approx \frac{\int_0^{70^\circ} \sin\theta_z d\theta_z}{\int_0^{\theta_{lim}} \sin\theta_z d\theta_z + (1 - f_o)\int_{\theta_{lim}}^{70^\circ} \sin\theta_z d\theta_z}, \tag{10}$$

$$F_o \approx \frac{1 - \cos 70^\circ}{1 - f_o \cos\theta_{lim} + (f_o - 1)\cos 70^\circ}. \tag{11}$$

For typical Tenerife values of $h_o \approx 9$ m, $d_o \approx 4$ m (i.e. about 8 m in diagonal between facing buildings), and $f_o \approx 0.9$. This leads to $\theta_{lim} \approx 24^\circ$ and then $F_o \approx 4.6$.

As said, the obstacle correction varies from one pixel to another. For that reason the above correction is very approximate. We know that the obstacle correction is independent of the wavelength. It should be the same for the three JC bands. The correction factors for the JC bands nominal wavelength are shown in table 3.

In this paper, we decided to use SB data acquired with ASTMON cameras during 2019 April (same month as for the VIIRS-DNB data), both in OT and ORM, to determine if our theoritical F_o estimate fit the observations and ultimately find a better value to use instead. The obstacles correction factor was empirically verified so that the total modelled zenith SB reduction upon a complete shutdown of the lights (see Table 8) fit with the measured SB differences in B and *V* bands between OT and ORM (see Table 1). This exercise led us to a value of $F_o = 5.05$ instead of 4.6 (i.e. 10 per cent larger). With that empirical value, we obtain a fit of *B* and *V* bands reductions that is within 0.02 mag arcsec^{-2}. Part of this correction can come from the fact that VIIRS-DNB data are not acquired at the same moment than SB measurements. But it is most probably coming from the use of only one set of obstacles values to estimate F_o that may not correctly represent the influence of all the pixels of the domain to the modelled SB. This is why we should implement the F_o correction directly to the input data in the future. The obstacle model used only assumes a single layer of uniform obstacles. But we assume that a more complete description such as the one made by Kocifaj (2018) could not provide a significant improvement to the correction of the VIIRS-DNB signal because of the relatively low zenith angles considered ($\theta_z \leq 70^\circ$).

The experimental determination of $F_o = 5.05$, was made using the difference in the 75 percentile (P75) values (see Table 1) SB in the *V* and *B* bands between the two sites. P75 values were estimated to provide the best proxy of the darkest conditions during 2019

Table 6. Fraction of the zenith artificial sky radiance to the total by municipality or area. Converted case stand for the change of all lighting devices of the protected area to PCamber with 20 per cent output flux reduction and the change of all lighting devices of the unprotected area to LED2700K with 70 per cent output flux reduction. The five most contributing municipalities to the present *V*-band radiance are in bold. We also indicate their decreasing order of importance in the *V* band before their names.

Municipality/zone	Protected area	Present			Fully converted		
		B $\theta_z = 0$ per cent	*V* $\theta_z = 0$ per cent	*R* $\theta_z = 0$ per cent	*B* $\theta_z = 0$ per cent	*V* $\theta_z = 0$ per cent	*R* $\theta_z = 0$ per cent
Adeje	yes	1.4	1.7	1.7	0.7	2.2	0.0
Arafo	no	4.6	3.7	3.6	4.6	2.1	1.7
Arico	no	5.4	6.0	6.1	6.9	3.2	2.6
Arona	mix	1.8	2.1	2.2	2.9	2.2	2.2
Buenavista	yes	0.0	0.0	0.0	0.0	0.1	0.1
Candelaria	no	3.7	4.2	4.2	6.0	2.7	2.2
Fasnia	no	2.3	2.9	2.9	4.3	1.9	1.6
Garachico	yes	0.2	0.2	0.2	0.1	0.3	0.4
5- Granadilla	no	6.2	**6.6**	6.7	8.5	4.1	3.4
La Laguna	mix	3.6	4.5	4.6	6.5	5.0	4.9
La Guancha	yes	1.0	1.1	1.1	0.4	1.3	1.5
Guia de Isora	yes	0.5	0.6	0.6	0.3	0.8	0.9
2- Güímar	no	10.8	**9.6**	9.4	12.8	5.8	4.7
Icod de los Vinos	yes	1.0	1.2	1.2	0.5	1.5	1.8
La Matanza	yes	0.5	0.9	0.9	1.0	1.5	1.6
1- La Orotava	yes	17.4	**16.7**	16.7	7.0	22.4	25.5
Puerto de la Cruz	yes	4.7	4.0	3.9	1.5	4.9	5.6
3- Los Realejos	yes	7.0	**9.0**	9.3	5.7	13.3	14.9
El Rosario	no	3.4	3.2	3.1	3.9	1.8	1.5
San Juan de la Rambla	yes	1.0	1.2	1.2	0.5	1.6	1.8
San Miguel	no	6.5	3.6	3.2	2.2	1.0	0.9
4- Santa Cruz de Tenerife	no	7.7	**6.9**	6.8	8.5	3.9	3.2
Santa Ursula	yes	1.6	1.9	2.0	0.9	2.7	3.1
Santiago del Teide	yes	0.1	0.2	0.2	0.4	0.5	0.5
Sauzal	yes	0.9	1.2	1.2	0.5	1.5	1.7
Los Silos	yes	0.1	0.1	0.1	0.0	0.1	0.1
Tacoronte	yes	0.6	1.4	1.5	1.3	2.3	2.6
El Tanque	yes	0.2	0.2	0.2	0.1	0.2	0.3
Tegeste	yes	0.3	0.4	0.4	0.2	0.6	0.6
La Victoria	yes	1.3	1.5	1.5	0.6	2.0	2.3
Vilaflor	no	0.3	0.3	0.3	0.3	0.1	0.1
Protected zone	yes	42.5	46.4	47.1	27.1	65.2	73.3
Unprotected zone	no	53.8	50.4	49.8	62.8	28.9	23.7
Tenerife	–	96.3	96.7	96.9	89.0	93.7	93.9
All	–	100.0	100.0	100.0	100.0	100.0	100.0
Artificial radiance W sr^{-1} m^{-2}		3.89E-08	2.20E-07	2.24E-07	1.29E-08	1.14E-07	1.16E-07

April. Using 99 percentile (P99) data should normally be better but, for the month of 2019 April, there was some contamination in the P99 band data that disappeared in the 75 percentile data. We assume that the SB at ORM in its best atmospheric conditions, is very close to the natural SB. This assumption should be true within 0.03 mag $arcsec^{-2}$ according to Benn & Ellison (1998). This assumption do not apply to the *R* band. We exclude the *R* band because that, on La Palma Island, many of the light fixtures are either low-pressure sodium or monochromatic amber LEDs. These artificial lights only emit in the *R* band. For that reason, we cannot assume that the *R* band SB at ORM is as representative of the natural SB as the *B* and *V* bands. Note that the exclusion of the *R* band only concern the estimation of the natural SB. The red part of the spectrum was considered for the modeling of the OT sky in other parts of our work. Table 2 show the P99 zenith SB recorded at ORM for the years 2018–2019. These measurements are brighter than the natural SB S_{bg} estimates made by Benn & Ellison (1998) in the *B* and *V* (-0.07 mag $arcsec^{-2}$ in B, -0.09 mag $arcsec^{-2}$ in V). But we recall that Benn & Ellison (1998) suggested to add 0.03 mag $arcsec^{-2}$ in all bands to determine the natural level. This is what we have done in *B* and *V*. Considering that, the new 2018–2019 measurements are consistent with the 1998 measurements in *B* and *V* bands. In the *R* band, the P99 measurement is darker than the Benn & Ellison (1998) estimate ($+0.15$ mag $arcsec^{-2}$). The ORM SB decrease in the *R* band since 1998 is probably due to the significant change in the lighting systems on La Palma. In 1998, there was a lot of Low Pressure Sodium lamps that are emitting in the *R* band. Then, we must admit that the natural SB evaluation made by Benn & Ellison (1998) in the *R* band was overestimated of at least 0.15 mag $arcsec^{-2}$. For that reason, we will use the 2018–2019 P99 data as the best estimate of S_{bg} in the *R* band while keeping the Benn & Ellison (1998) values for *B* and *V* bands.

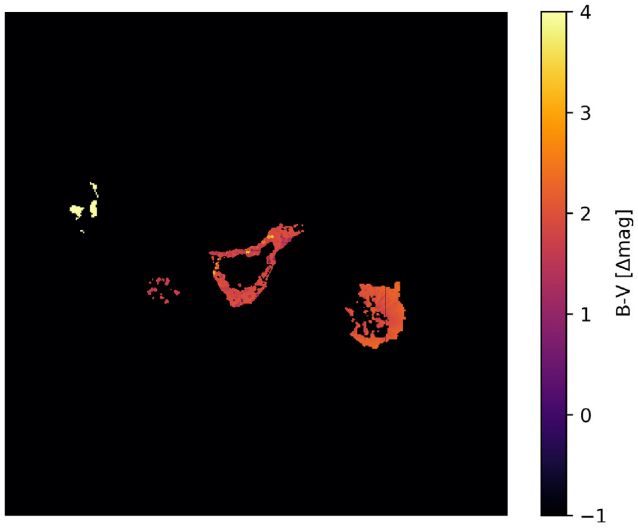

Figure 8. Colour index of the artificial sky brightness of the different parts of the Canary Islands to the artificial zenith sky radiance at OT.

Table 7. Comparison of the artificial radiances after mid-night for the present situation and the full conversion.

Band	θ_z	Present radiance (W sr^{-1} m^{-2})	Converted radiance (W sr^{-1} m^{-2})	Converted/present
B	0	3.89E-08	1.29E-08	0.33
V	0	2.20E-07	1.14E-07	0.52
R	0	2.24E-07	1.16E-07	0.52
B	30 avg	4.68E-08	1.50E-08	0.32
V	30 avg	2.68E-07	1.36E-07	0.51
R	30 avg	2.73E-07	1.42E-07	0.52

2.5 Conversion from radiance to SB

Illumina calculates only the artificial sky radiance. To determine the total SB equivalent in units of mag arcsec^{-2} it is mandatory to get a good estimate of the natural component of the SB for the site and period. The natural SB is highly variable with time, altitude, season, and observing direction. It is composed of light from multiple sources such as the zodiacal light, the starlight, the sky glow, and the Milky Way (Benn & Ellison 1998). In this study, we are using natural SB estimates made by Benn & Ellison (1998) to determine the background SB and radiance. This natural SB excludes starlight. For that reason, the ASTMON measurements are shifted compared to the background SB, but the shift is the same for both OT and ORM when considering the same period. This is why we used the SB differences between the two sites instead of absolute values to calibrate the model results as explained in Section 2.4.

For a given JC band, let's call the radiance responsible for the natural contribution without starlight, the background radiance (R_{bg}). We also define R_a as the artificial component of the radiance, and R as the total sky radiance excluding starlight. The total radiance is defined as $R = R_a + R_{bg}$. According to the definition of the magnitude, we can write

$$R_{bg} = R_0 10^{-0.4 S_{bg}}. \tag{12}$$

The zero-point radiances R_0 are obtained from Bessell (1979) and given in Table 4. They were derived with the relative absolute energy distribution of Hayes (1970) standards and the absolute flux calibration for α Lyrae given by Hayes & Latham (1975). Values of R_{bg} and corresponding S_{bg} measurements (Benn & Ellison (1998) in *B* and *V* bands and ASTMON in the *R* band) are given in Table 5 for OT in 2019 April.

Once R_{bg} is known, the SB from any modelled artificial radiance integrated over the JC band (R_a) can be determined from the definition of the magnitude:

$$S = -2.5 \log \left(\frac{R_a + R_{bg}}{R_0} \right). \tag{13}$$

R_a have to be determined by integrating the modelled artificial radiances for the spectral bins over the JC band. In a similar way, we can express the variation in SB (ΔS) after a shutdown or after a reduction of the radiance of a given area (ΔR_a):

$$\Delta S = -2.5 \log \left(\frac{R_a - \Delta R_a + R_{bg}}{R_a + R_{bg}} \right). \tag{14}$$

Equation (14) is used to calculate the values of Tables 8 and 9. For the case of a lamp conversion, ΔR_a is the difference in artificial radiance contribution of an area (present situation minus converted). For a complete shutdown of an area, ΔR_a is simply the present artificial radiance contribution of the area.

3 RESULTS AND ANALYSIS

Fig. 6 shows the relative importance of the different part of the modelling domain in terms of their contribution to the zenith artificial radiance in the *V* band. On that figure, it is noticeable that most of the zenith artificial radiance at OT is coming from the island of Tenerife itself. The second contributor is Gran Canaria, and the third is the small island of La Gomera. The contribution of La Palma island is negligible. We did not calculate the effect of El Hierro but it is for sure a lot smaller. The low contribution of La Palma is easy to explain because of its modest lighting infrastructure combined to its large distance from Tenerife. Fig. 7 gives more details about the contribution of different parts of the Island of Tenerife. In this figure, we can clearly perceive that the contribution is a complex combination of the distance to OT and the installed lamp fluxes. It can be noticed for example that Santa Cruz de Tenerife is not a huge contributor even if it emits a large amount of light as seen from Fig. 4. A more detailed view of that information is given in Table 6. In this table, the percentage of the total artificial radiance is given for each municipality and protected/unprotected areas. This table shows that towards zenith in the *V* band and for the present situation, 97 per cent of the observed radiance comes from Tenerife Island (only 3 per cent comes from the other islands). The most contributing municipality is La Orotava with around 17 per cent followed by Güímar with around 11 per cent. The protected area contributes to about 43 per cent while it is about 54 per cent for the unprotected area. The capital Santa Cruz is not the most important contributor with about 7 per cent. Another interesting result is that Los Cristianos and Playa de Las Américas (Arona), highest density tourists areas, contributes with about 2 per cent. Some of these contributions may appear low and counter intuitive. This is because that our feeling of light pollution levels on site is driven by the observation of light domes towards the main sources. Here, we show that their contributions are relatively low when looking towards zenith.

In the advent of a complete conversion to LED, these numbers change a bit. The contribution of other islands becomes relatively more important (between 6 per cent and 11 per cent) but not in absolute values since in this conversion scenario only Tenerife is converted. After conversion, the relative contribution of Güímar is

Table 8. Reduction of the sky brightness after midnight in the *B, V, R* JC bands if a municipality or area is totally shutdown. The five most contributing municipalities to the present *V*-band SB are in bold. We also indicate their decreasing order of importance in the *V* band before their names.

Municipality/zone	Protected area	B $\theta_z = 0$ (mag arcsec^{-2})	V $\theta_z = 0$ (mag arcsec^{-2})	R $\theta_z = 0$ (mag arcsec^{-2})	B $\theta_z = 30^o$ (mag arcsec^{-2})	V $\theta_z = 30^o$ (mag arcsec^{-2})	R $\theta_z = 30^o$ (mag arcsec^{-2})
Adeje	Yes	0.002	0.009	0.006	0.003	0.010	0.007
Arafo	No	0.008	0.020	0.012	0.009	0.022	0.013
Arico	No	0.009	0.032	0.020	0.011	0.035	0.023
Arona	Mix	0.003	0.011	0.007	0.004	0.013	0.008
Buenavista	Yes	0.000	0.000	0.000	0.000	0.000	0.000
Candelaria	No	0.006	0.022	0.014	0.007	0.024	0.016
Fasnia	No	0.004	0.015	0.010	0.005	0.016	0.011
Garachico	Yes	0.000	0.001	0.001	0.000	0.001	0.001
5- Granadilla	No	0.011	**0.035**	0.022	0.013	0.040	0.026
La Laguna	Mix	0.006	0.024	0.015	0.007	0.027	0.018
La Guancha	Yes	0.002	0.006	0.004	0.002	0.006	0.004
Guia de Isora	Yes	0.001	0.003	0.002	0.001	0.003	0.002
2- Güímar	No	0.018	**0.051**	0.031	0.021	0.054	0.034
Icod de los Vinos	Yes	0.002	0.006	0.004	0.002	0.007	0.005
La Matanza	Yes	0.001	0.005	0.003	0.001	0.005	0.003
1- La Orotava	Yes	0.030	**0.087**	0.054	0.034	0.092	0.059
Puerto de la Cruz	Yes	0.008	0.021	0.013	0.009	0.023	0.015
3- Los Realejos	Yes	0.012	**0.048**	0.030	0.013	0.050	0.033
El Rosario	No	0.006	0.017	0.010	0.007	0.019	0.012
San Juan de la Rambla	Yes	0.002	0.006	0.004	0.002	0.007	0.004
San Miguel	No	0.011	0.019	0.011	0.013	0.022	0.013
4- Santa Cruz de Tenerife	No	0.013	**0.037**	0.022	0.016	0.042	0.027
Santa Ursula	Yes	0.003	0.010	0.007	0.003	0.012	0.008
Santiago del Teide	Yes	0.000	0.001	0.001	0.000	0.001	0.001
Sauzal	Yes	0.002	0.006	0.004	0.002	0.007	0.005
Los Silos	Yes	0.000	0.000	0.000	0.000	0.001	0.000
Tacoronte	Yes	0.001	0.007	0.005	0.001	0.008	0.006
El Tanque	Yes	0.000	0.001	0.001	0.000	0.001	0.001
Tegeste	Yes	0.000	0.002	0.001	0.001	0.002	0.001
La Victoria	Yes	0.002	0.008	0.005	0.003	0.009	0.006
Vilaflor	No	0.000	0.002	0.001	0.001	0.002	0.001
Protected zone	Yes	0.071	0.226	0.146	0.081	0.243	0.163
Unprotected zone	No	0.089	0.243	0.154	0.104	0.266	0.175
Tenerife	–	0.155	0.427	0.281	0.178	0.461	0.316
All	–	0.160	0.439	0.289	0.184	0.474	0.325

reduced, while Los Realejos increase significantly to become the second contributing municipality. This is because that a part of Los Realejos is already converted to PCamber in the present situation, so that its absolute contribution is less reduced after the conversion in comparison to other municipalities.

Figs 8 and 9 show the $B - V$ colour index in magnitude calculated using the artificial radiances only. These figures are for the present situation. It is clear on Fig. 8 that La Palma does not have much blue light ($B - V \approx 4$), but there are also some low blue content spots on the island of Tenerife (Fig. 9), Los Realejos being one of them. These low blue radiance spots are places mostly already converted to PCamber.

Table 7 shows the total artificial radiances in *B*, *V*, and *R* at zenith angles $\theta_z = 0^\circ$ and $\theta_z = 30^\circ$ for the present situation and for the conversion scenario. The zenith artificial radiance after conversion is ≈33 per cent of its present value in the *B* band, while it is around 52 per cent in the two other filters. This result shows clearly that the blue content of the SB is more efficiently reduced after conversion but the reduction is also significant in the *V* and *R* bands (about a factor of 2). These reductions are the result of a combination of the change in colour of the lamp spectra and a general reduction of the upward emitted light since the LED fixture used for the conversion have an upward light output ratio (ULOR) of 0.

One interesting aspect of modelling the SB is that we can a test unlimited number of changes in the lighting infrastructure and environmental variables to determine their effects on the SB. Table 8 shows the SB change associated with the shutdown of each municipality. This table shows that a complete shutdown of Tenerife Island would improve zenith OT SB by 0.155 mag arcsec^{-2} in the *B* band, 0.427 mag arcsec^{-2} in the *V* band and 0.258 mag arcsec^{-2} in the *R* band. These numbers are the maximal SB reductions availables but implies a complete shutdown of the light fixtures. That is certainly not realistic in the real world. With such a SB reduction, OT sky would be as dark as ORM sky. The five most contributing municipalities to the zenith SB in *V* band are in order of decreasing importance: La Orotava, Güímar, Los Realejos, Santa Cruz de Tenerife and Granadilla. The SB reductions at $\theta_z = 30^\circ$ are even larger (e.g. 0.461 mag arcsec^{-2} in the *V* band).

A more realistic scenario is presented in Tables 9 and 10. Table 9 shows the expected SB reduction after a conversion of a municipality or area to the relevant LED technology. As shown in the table, no gain in zenith SB may be achieved with the lighting conversion

Table 9. Reduction of the sky brightness after midnight in the *B, V, R, JC* bands if a municipality or area is converted to LED. PCamber with 20 per cent output flux reduction in the protected area and LED2700K with 70 per cent output flux reduction in the unprotected area. Output flux assumed to remain constant for other islands. The five municipalities with the largest reduction of the *V*-band SB after a conversion to LED are in bold. We also indicate their decreasing order of importance in the V band before their names. Note that the order is different from Tables 6 and 8.

Municipality/zone	Protected area	B $\theta_z = 0$ (mag arcsec^{-2})	V $\theta_z = 0$ (mag arcsec^{-2})	R $\theta_z = 0$ (mag arcsec^{-2})	B $\theta_z = 30^o$ (mag arcsec^{-2})	V $\theta_z = 30^o$ (mag arcsec^{-2})	R $\theta_z = 30^o$ (mag arcsec^{-2})
Adeje	yes	0.002	0.003	0.006	0.002	0.002	0.001
Arafo	no	0.005	0.014	0.009	0.005	0.010	0.008
5- Arico	no	0.005	**0.024**	0.016	0.005	0.017	0.013
Arona	mix	0.001	0.005	0.003	0.002	0.004	0.003
Buenavista	yes	0.000	0.000	0.000	0.000	0.000	0.000
Candelaria	no	0.003	0.015	0.010	0.003	0.010	0.008
Fasnia	no	0.002	0.010	0.007	0.002	0.007	0.006
Garachico	yes	0.000	0.000	0.000	0.000	0.000	0.000
4- Granadilla	no	0.006	**0.025**	0.016	0.006	0.018	0.014
La Laguna	mix	0.002	0.010	0.007	0.004	0.008	0.006
La Guancha	yes	0.001	0.002	0.001	0.001	0.002	0.001
Guia de Isora	yes	0.001	0.001	0.000	0.001	0.001	0.000
1- Güímar	no	0.011	**0.036**	0.023	0.011	0.025	0.019
Icod de los Vinos	yes	0.001	0.002	0.001	0.002	0.001	0.001
La Matanza	yes	0.000	0.001	0.000	0.000	0.000	0.000
2- La Orotava	yes	0.026	**0.028**	0.011	0.025	0.019	0.010
Puerto de la Cruz	yes	0.007	0.008	0.003	0.007	0.006	0.003
Los Realejos	yes	0.009	0.012	0.005	0.008	0.008	0.004
El Rosario	no	0.004	0.012	0.008	0.004	0.009	0.007
San Juan de la Rambla	yes	0.002	0.002	0.001	0.001	0.001	0.001
San Miguel	no	0.010	0.017	0.009	0.010	0.012	0.008
3- Santa Cruz de Tenerife	no	0.008	**0.027**	0.017	0.009	0.020	0.015
Santa Ursula	yes	0.002	0.003	0.001	0.002	0.002	0.001
Santiago del Teide	yes	0.000	0.000	0.000	0.000	0.000	0.000
Sauzal	yes	0.001	0.002	0.001	0.001	0.001	0.001
Los Silos	yes	0.000	0.000	0.000	0.000	0.000	0.000
Tacoronte	yes	0.000	0.001	0.000	0.000	0.001	0.000
El Tanque	yes	0.000	0.001	0.000	0.000	0.000	0.000
Tegeste	yes	0.000	0.000	0.000	0.000	0.000	0.000
La Victoria	yes	0.002	0.003	0.001	0.002	0.002	0.001
Vilaflor	no	0.000	0.001	0.001	0.000	0.001	0.001
Protected zone	yes	0.059	0.071	0.030	0.058	0.050	0.025
Unprotected zone	no	0.058	0.211	0.132	0.058	0.147	0.112
Tenerife	–	0.122	0.299	0.172	0.121	0.205	0.141
All	–	0.122	0.299	0.172	0.122	0.208	0.144

of other islands to PCamber. Furthermore, only a tiny reduction ($\leq$0.002 mag arcsec^{-2}) can be obtained at 30° zenith angle from the conversions of the other islands. The five municipalities conversion that may deliver the maximum zenith *V*-band SB reduction are, in order of decreasing effect, (1) Güímar (pop. 20 190), (2) La Orotava (pop. 42 029), (3) Santa Cruz de Tenerife (pop. 207 312), (4) Granadilla (pop. 50 146), (5) Arico (pop. 7 988). The available SB reduction is relatively similar from one to the other municipality with 0.036 mag arcsec^{-2} for Güímar and 0.025 mag arcsec^{-2} for Arico. Some of these five municipalities are clearly less populated and thus involve less light points to be converted. These municipalities should be prioritized to get the maximum SB reduction with minimal investment. The ratio of total sky radiance reduction per inhabitant for each municipality is shown in Table 10. If we consider the maximum zenith sky radiance reduction for minimal investment in *V* band, Fasnia should certainly be the best starting point followed by Arico, Arafo, Güímar and San Miguel. These five municipalities may reduce the total *V*-band sky radiance by 9.2 per cent with only 6.25 per cent of the Tenerife population, compared to the complete conversion o the island that should result in a radiance reduction of 24.1 per cent.

In terms of SB, the complete conversion of the Tenerife Island should improve the zenith *V*-band SB by 0.299 mag arcsec^{-2}. This is actually the best SB reduction in the *V* band that can be achieved with the lighting conversion rules currently in place. The conversion of the five municipalities listed above should deliver a SB reduction of $\approx$0.1 mag arcsec^{-2} in the *V* band.

4 CONCLUSIONS

In this paper, we show how a radiative transfer code dedicated to the modelling of the sky radiance can be used to plan an efficient light conversion to restore the night SB to its natural value. The methodology presented is applied to the case of OT, Tenerife. We showed how the determination of the sky radiance for the present situation and for some LED conversion plans can be combined to optimize the night sky darkness restoration. As for now, we do not have the experimental data to validate the accuracy of the modeled results. This will only be possible when a municipality identified as an important contributor to the SB will be completely converted to LEDs. We estimate that the main source of errors in that study is

Table 10. Relative reduction of the total zenith sky radiances (artificial + natural) in the *B, V, R* bands and equivalent reduction per inhabitant (INE 2019). The municipalities in bold are the five most efficient to reduce the zenith *V*-band sky brightness when considering the investment per inhabitant. We estimate that the replacement program should focus first on that list of municipalities.

Municipality/zone	Population	Relative reduction B $\theta_z = 0$ per cent	V $\theta_z = 0$ per cent	R $\theta_z = 0$ per cent	Relative reduction per inhabitant B $\theta_z = 0$ per cent per inhabitant $\times 10^6$	V $\theta_z = 0$ per cent per inhabitant $\times 10^6$	R $\theta_z = 0$ per cent per inhabitant $\times 10^6$
Adeje	47869	0.19	0.3	0.5	4.0	5.3	10.8
3- Arafo	5551	0.49	1.3	0.8	87.9	**237.5**	149.6
2- Arico	7988	0.49	2.1	1.4	61.5	**268.6**	179.8
Arona	81216	0.13	0.5	0.3	1.6	6.0	3.9
Buenavista	4778	0.00	0.0	0.0	1.0	1.0	0.4
Candelaria	27985	0.27	1.4	0.9	9.7	49.0	33.2
1- Fasnia	2786	0.15	0.9	0.6	52.1	**333.7**	230.5
Garachico	4871	0.02	0.0	0.0	4.6	5.3	2.1
Granadilla	50146	0.54	2.3	1.5	10.8	45.0	29.9
La Laguna	157503	0.23	0.9	0.6	1.4	5.9	3.9
La Guancha	5520	0.14	0.2	0.1	24.8	36.2	17.9
Guia de Isora	21368	0.06	0.1	0.0	2.8	3.4	1.4
4- Güímar	20190	1.03	3.3	2.1	51.2	**162.4**	105.4
Icod de los Vinos	23254	0.14	0.2	0.1	5.9	7.9	3.6
La Matanza	9061	0.03	0.0	0.0	3.5	5.4	2.7
La Orotava	42029	2.40	2.5	1.1	57.1	60.6	25.0
Puerto de la Cruz	30468	0.67	0.7	0.3	22.0	23.4	9.8
Los Realejos	36402	0.81	1.1	0.5	22.3	29.0	13.0
El Rosario	17370	0.34	1.1	0.7	19.5	64.3	41.6
San Juan de la Rambla	4828	0.14	0.2	0.1	28.8	36.7	16.5
5- San Miguel	20886	0.92	1.5	0.9	44.2	**73.3**	40.8
Santa Cruz de Tenerife	207312	0.77	2.4	1.6	3.7	11.8	7.5
Santa Ursula	14679	0.21	0.3	0.1	14.5	18.0	8.0
Santiago del Teide	11111	0.00	0.0	0.0	0.0	0.0	0.0
Sauzal	8934	0.12	0.2	0.1	13.9	20.9	10.3
Los Silos	4693	0.01	0.0	0.0	2.2	3.2	1.6
Tacoronte	24134	0.03	0.1	0.0	1.4	3.1	1.7
El Tanque	2763	0.03	0.1	0.0	11.5	20.0	10.7
Tegeste	11294	0.04	0.0	0.0	3.2	3.5	1.3
La Victoria	9185	0.17	0.2	0.1	19.0	25.7	12.1
Vilaflor	1667	0.03	0.1	0.1	16.3	64.4	42.7
Protected zone	–	5.32	6.3	2.8	–	–	–
Unprotected zone	–	5.24	17.6	11.5	–	–	–
Tenerife	917841	10.61	24.1	14.7	11.6	26.2	16.0
All	–	10.61	24.1	14.7	–	–	–
Total radiance $Wm^{-2}sr^{-1}$		2.45E-07	4.42E-07	7.34E-07	–	–	–

coming from the present situation lighting inventory that may not be as accurate as it should. But such errors will not change dramatically the conclusions drawn in this study.

The integration of the results according to the *JC* bands spectral responses and for defined territories (like municipality limits) render it possible to identify the most urgent municipalities to convert to get the maximum decrease of the SB with the minimum financial and human resources.

We demonstrated that just the completion of the undergoing lighting infrastructure conversion plan of the Tenerife Island should translate into a *V*-band SB reduction of $\approx$0.3 mag arcsec^{-2}. Such improvement would not be enough to recover a sky darkness typical of astronominal sites like Observatorio del Roque de los Muchachos, however, it is not that far from it. We would need a zenith *V*-band SB reduction of $\approx$0.44 mag arcsec^{-2} to be reaching the same sky darkness. A reduction of $\approx$0.3 mag arcsec^{-2} means a reduction of the total *V*-band sky radiance by 24 per cent and a reduction of the artificial *V*-band sky radiance by 48 per cent. This is actually a dramatic reduction of the light pollution. A complete shutdown of the Tenerife light would improve the *V*-band zenith SB by $\approx$0.43 mag arcsec^{-2}.

The capital Santa Cruz de Tenerife and the busy tourist places of Los Cristianos and Playa de Las Américas (Arona) are producing, respectively, 7 per cent and 2 per cent of the artificial sky radiance towards zenith. Their contribution would be dominant when looking closer to horizon in their respective directions but it was not evaluated in this study. Actually, our results show clearly that nearby sources are the main contributors to the SB towards zenith at OT. We can expect that, for some specific research applications needing to observe closer to horizon, it can represent an important problem and then any further

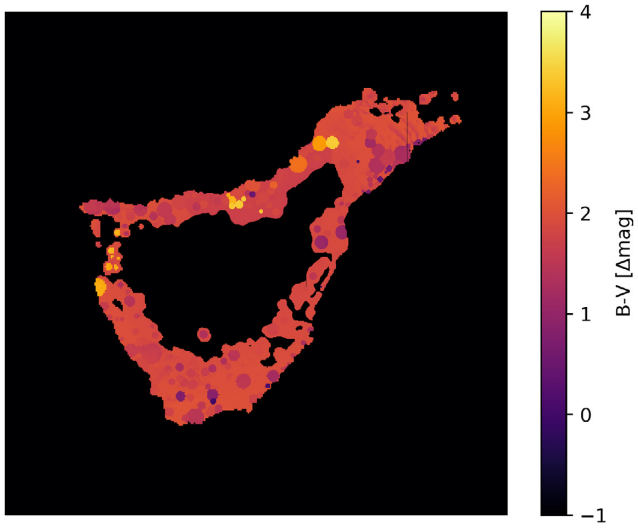

Figure 9. Colour index of the artificial sky brightness of the different parts of the Tenerife Island to the artificial zenith sky radiance at OT.

touristic development should consider strong mitigation measures to restrict their light pollution emissions.

We also showed that the sky radiance reduction per inhabitant can be an efficient proxy to optimize SB reductions with limited resources. Applying the conversion plan for the five municipalities showing the highest ratio of radiance reduction per inhabitant (see Table 10) allows the reduction of the SB by ≈0.1 mag arcsec^{-2} (i.e. a total *V*-band sky radiance reduction of ≈9 per cent compared to the maximum available of ≈24 per cent). But these municipalities represent only about 6 per cent of the Tenerife population.

This study showed how the atmospheric correction and, most importantly, the obstacles blocking correction play significant role in determining the lamp fluxes from the VIIRS-DNB radiances. For that reason, we will emphasize the addition of this feature to the Illumina model.

ACKNOWLEDGEMENTS

We applied the sequence-determines-credit approach (Tscharntke et al. 2007) for the sequence of authors. An important part of that research funded by M. Aubé's Fonds de Recherche du Québec - Nature et Technologies grant. Most computations were carried out on the Mammouth Parallel II cluster managed by Calcul Québec and Compute Canada. The operation of these supercomputers is funded by the Canada Foundation for Innovation, and the Fonds de Recherche du Québec - Nature et Technologies. Thanks to Julio A. Castro Almazán for his help in processing the ASTMON data. This study was carried out in part at IAC, we want to thank that institution and its deputy director for the financial support and warm welcome. Finally we want to thank our anonymous referee who did a very useful review that helped improving this work.

DATA AVAILABILITY

The data underlying this article will be shared on reasonable request to the corresponding author.

REFERENCES

Aceituno J., Sánchez S. F., Aceituno F. J., Galadí-Enríquez D., Negro J. J., Soriguer R. C., Gomez G. S., 2011, PASP, 123, 1076
Aubé M., 2007, in Marin C., ed., Proceedings of Starlight 2007 conference. La Palma, Spain
Aubé M., 2015, Phil. Trans. R. Soc. B, 370
Aubé M., Kocifaj M., 2012, MNRAS, 422, 819
Aubé M., Simoneau A., 2018, J. Quant. Spectrosc. Radiat. Transfer, 211, 25
Aubé M., Franchomme-Fossé L., Robert-Staehler P., Houle V., 2005, in Optics & Photonics 2005, San Diego USA, p. 589012
Aubé M., Fortin N., Turcotte S., García B., Mancilla A., Maya J., 2014, PASP, 126, 1068
Baddiley C., 2007, Br. Asron. Assoc., 345
Baldridge A. M., Hook S., Grove C., Rivera G., 2009, Remote Sens. Environ., 113, 711
Bara S., Lima R., 2018, Int. J. Sustainable Light., 20, 51
Benn C., Ellison S., 1998, Technical report, La Palma Tech, Note 115. Isaac Newton Group of Telescopes, La Palma
Berry R. L., 1976, J. R. Astron. Soc. Canada, 70, 97
Bertiau F. C., de Graeve E., Treanor P. J., 1973, Vatican obs. publ.
Bessell M., 1979, PASP, 91, 589
Cinzano P., Falchi F., 2013, MNRAS, 427, 3337
de Santamaría Antón S. S., 2017, Real decreto 580/2017, de 12 de junio, por el que se modifica el real decreto 243/1992, de 13 de marzo, por el que se aprueba el reglamento de la ley 31/1988, de 31 de octubre, sobre protección de la calidad astronómica de los observatorios del instituto de astrofísica de canarias, King of Spain, Madrid
Díaz-Castro F. J., 1998, New Astron. Rev., 42, 509
Elvidge C. D., Baugh K. E., Dietz J. B., Bland T., Sutton P. C., Kroehl H. W., 1999, Remote Sens. Environ., 68, 77
Elvidge C. D., Baugh K., Zhizhin M., Hsu F. C., Ghosh T., 2017, Int. J. Remote Sens., 38, 5860
Falchi F., 2011, MNRAS, 412, 33
Falchi F. et al., 2016, Sci. Adv., 2, e1600377
Garstang R. H., 1986, PASP, 98, 364
Gómez V. Z., 1992, Ley 31/1988, de 31 de octubre, sobre protección de la calidad astronómica de los observatorios del instituto de astrofísica de canarias. King of Spain, Madrid
Hayes D., 1970, ApJ, 159, 165
Hayes D. S., Latham D., 1975, ApJ, 197, 593
Holben B. N. et al., 1998, Remote Sens. Environ., 66, 1
Imhoff M. L., Lawrence W. T., Stutzer D. C., Elvidge C. D., 1997, Remote Sens. Environ., 61, 361
INE, 2019, Instituto nacional de estadística, population estimate of 1 january 2019, INE, Madrid, Spain
Juan Carlos R. D. E., I, 1988, Ley 31/1988, de 31 de octubre, sobre protección de la calidad astronómica de los observatorios del instituto de astrofísica de canarias. King od Spain, Madrid
Kneizys F. X., Sheitle E. P., Gallery W., Chetwynd J. H., Abreu J. L. W., Selby J. E. A., Fenn R. W., Mcclatchey R. A., 1980, Technical Report 697, Atmospheric Transmittance/Radiance: Computer Code LOWTRAN 5. Optical Physics Division, Air Force Geophysics Laboratory, Air Force Geophysics laboratory Hanscom Air Force Base, MA, USA
Kocifaj M., 2007, Appl. Opt., 46, 3013
Kocifaj M., 2018, J. Quant. Spectrosc. Radiat. Transfer, 205, 253
Kyba C. C. et al., 2015, Sci. Rep., 5
Luginbuhl C. B., Duriscoe D. M., Moore C. W., Richman A., Lockwood G. W., Davis D. R., 2009, PASP, 121, 204
Masek J. G. et al., 2006, IEEE Geosci. Remote Sens. Lett., 3, 68
Munoz-Tunón C., 2002, in Astronomical Site Evaluation in the Visible and Radio Range. p. 498
Munoz-Tunón C., Vernin J., Varela A., 1997, A&AS, 125, 183
Patat F., 2008, A&A, 481, 575
Pérez-Jordán G., Castro-Almazán J., Muñoz-Tuñón C., Codina B., Vernin J., 2015, MNRAS, 452, 1992
Pun C. S. J., So C. W., 2012, Environ. Monit. Assess., 184, 2537

Pun C. S. J., So C. W., Leung W. Y., Wong C. F., 2014, J. Quant. Spectrosc. Radiat. Transfer, 139, 90
Puschnig J., Posch T., Uttenthaler S., 2014, J. Quant. Spectrosc. Radiat. Transfer, 139, 64
Sánchez de Miguel A., 2015, PhD thesis, Universidad Complutense de Madrid
Sánchez de Miguel A., Aubé M., Zamorano J., Kocifaj M., Roby J., Tapia C., 2017, MNRAS, 467, 2966
Ścieżor T., 2020, J. Quant. Spectrosc. Radiat. Transfer, 247, 106962
Shettle E. P., Fenn R. W., 1979, Environ. Res. Papers, 676, 89
Treanor P. J., 1973, The Observatory, 93, 117
Tscharntke T., Hochberg M. E., Rand T. A., Resh V. H., Krauss J., 2007, PLoS Biol., 5, e18
Vernin J., Muñoz-Tuñón C., 1992, A&A, 257, 811
Vernin J., Munoz-Tunon C., 1994, A&A, 284, 311
Vernin J. et al., 2011, PASP, 123, 1334

APPENDIX A: LIGHT FIXTURE AND OBSTACLES INVENTORY FOR THE PRESENT SITUATION

Table A1. Light fixture and obstacles inventory.

Latitude (deg)	Longitude (deg)	Radius (km)	Obst. height (m)	Obst. distance (m)	Obst. filling factor –	Lamp height (m)	Lamp spectra and ULOR
28.30094	−16.510816	49.97	5	7	0.2	6	100_HPS_0
27.93533	−15.598841	35.15	15	15	0.9	6	90_HPS_2 10_L40_0
28.66761	−17.848418	25.76	15	12	0.95	6	15_PCA_0 10_HPS_0 75_LPS_0
28.46752	−16.592312	19.5	6	10	0.2	5	100_HPS_2
28.24940	−16.814967	19.27	8	35	0.1	9	100_HPS_0
28.63933	−16.359244	17.11	8	35	0.1	9	100_HPS_0
28.12460	−17.230469	14.59	7	15	0.8	6	90_HPS_2 10_L40_0
28.33264	−16.396496	5.07	5	100	0.1	9	100_HPS_0
28.04566	−16.575587	2.44	13	100	0.25	9	100_HPS_0
28.51875	−16.387880	2.08	6	30	0.4	7	99_HPS_0 1_PCA_0
28.12210	−16.734982	1.97	12	18	0.7	9	100_HPS_0
28.37376	−16.851106	1.95	10	10	0.9	6	100_HPS_0
28.08387	−16.732077	1.79	16	28	0.6	8	10_PCA_0 2_L27_0 78_HPS_0
28.01340	−16.649815	1.73	14	12	0.9	6	80_HPS_0 15_MV3_0 5_PCA_0
28.51767	−16.300309	1.723	6	25	0.3	6	100_HPS_0
28.44829	−16.458228	1.71	8	30	0.5	7	50_PCA_0 50_HPS_1
28.23371	−16.841736	1.69	16	22	0.7	7	97_PCA_0 3_L27_0
28.46672	−16.256862	1.68	24	30	0.9	9	90_HPS_0 5_L40_0 5_MH_1
28.42892	−16.493302	1.67	24	30	0.7	6	100_HPS_0
28.10089	−16.755249	1.67	12	30	0.6	9	100_HPS_0
28.37183	−16.815418	1.62	8	10	0.9	4	100_HPS_3
28.44793	−16.305677	1.59	9	11	0.9	5	95_HPS_0 5_MH_1
28.46175	−16.285635	1.56	32	16	0.75	6	95_HPS_0 5_MH_1
28.39869	−16.572359	1.49	5	30	0.8	4	100_HPS_0
28.41183	−16.545088	1.49	20	15	0.8	7	60_PCA_0 21_L27_0 19_HPS_0
28.36733	−16.714263	1.47	24	7	0.9	4	100_HPS_0
28.48344	−16.416816	1.45	8	30	0.5	3	80_PCA_0 20_HPS_0
28.07720	−16.557724	1.41	8	10	0.9	7	100_HPS_0
28.46759	−16.379026	1.38	8	40	0.4	9	100_HPS_0
28.33341	−16.370738	1.38	7	50	0.85	10	90_HPS_0 2_L40_0 8_MH_5
28.37304	−16.785446	1.37	8	25	0.4	8	100_HPS_0
28.02369	−16.615692	1.33	10	26	0.7	5	100_HPS_0
28.05784	−16.731080	1.32	14	40	0.75	9	10_PCA_0 2_L27_0 78_HPS_0
28.36792	−16.760711	1.32	7	6	0.9	6	50_HPS_0 50_HPS_1
28.48450	−16.341955	1.31	5	60	0.5	9	100_HPS_0
28.31567	−16.411176	1.31	10	16	0.85	6	95_HPS_0 3_HPS_5 2_MH_20
28.12714	−16.774962	1.3	5	25	0.75	4	25_HPS_3 5_HPS_50 70_HPS_0
28.47380	−16.304124	1.28	12	10	0.9	9	95_HPS_0 5_MH_1
28.37888	−16.686270	1.28	9	15	0.7	5	100_HPS_0
28.48549	−16.391648	1.18	9	17	0.5	5	100_PCA_0
28.16630	−16.501999	1.16	5	8	0.8	7	90_HPS_0 10_HPS_1
28.44652	−16.264041	1.16	5	18	0.8	7	95_HPS_2 2.5_MH_2 2.5_FLU_2
28.05080	−16.711846	1.15	16	60	0.6	9	10_PCA_0 2_L27_0 78_HPS_0
28.08682	−16.500563	1.14	8	65	0.3	9	5_MH_10 95_HPS_0
28.52364	−16.344300	1.14	7	12	0.7	7	100_HPS_0
28.35083	−16.703138	1.12	7	10	0.5	7	50_HPS_3 50_HPS_0
28.05334	−16.616540	1.1	8	35	0.6	9	5_MH_10 95_HPS_0

Table A1 – *continued*

Latitude (deg)	Longitude (deg)	Radius (km)	Obst. height (m)	Obst. distance (m)	Obst. filling factor –	Lamp height (m)	Lamp spectra and ULOR
28.56943	−16.324811	1.1	8	6	0.6	7	95_HPS_0 3_PCA_0 2_L27_0
28.39099	−16.523835	1.09	9	12	0.9	5	100_HPS_0
28.48621	−16.318925	1.08	18	12	0.9	9	75_HPS_0 10_L40_0 10_L30_0
28.12130	−16.576724	1.08	10	20	0.9	6	3_HPS_38 97_HPS_0
28.21147	−16.778658	1.07	8	5	0.9	4	50_HPS_0 50_HPS_3
28.50047	−16.317123	1.05	7	12	0.6	5	90_HPS_0 10_L40_0
28.36897	−16.368080	1.03	8	30	0.8	6	100_HPS_0
28.46480	−16.403630	1.03	9	15	0.7	6	100_HPS_0
28.49336	−16.201951	0.98	6	35	0.4	8	95_HPS_0 2.5_MH_2 2.5_FLU_2
28.04623	−16.537383	0.97	20	15	0.8	7	100_HPS_0
28.07029	−16.655582	0.97	8	15	0.75	9	100_HPS_0
28.12996	−16.754614	0.96	13	10	0.8	9	100_HPS_0
28.02337	−16.698863	0.96	6	18	0.8	6	100_HPS_0
28.44967	−16.368691	0.94	8	10	0.6	7	100_HPS_0
28.35613	−16.780046	0.94	8	20	0.8	6	30_HPS_1 70_HPS_1
28.14254	−16.756250	0.93	5	12	0.4	6	100_HPS_0
28.05023	−16.678293	0.92	16	12	0.7	8	10_MH_5 90_HPS_0
28.53401	−16.361629	0.91	9	8	0.8	7	99_HPS_0 1_PCA_0
28.48467	−16.225677	0.91	6	100	0.1	7	30_HPS_0 70_L40_0
28.20192	−16.827965	0.9	15	25	0.8	9	100_HPS_0
28.49411	−16.372853	0.89	8	25	0.5	7	100_HPS_0
28.07346	−16.671971	0.89	8	10	0.8	7	100_HPS_0
28.08931	−16.658905	0.87	9	12	0.75	5	100_HPS_0
28.37785	−16.552871	0.85	9	10	0.9	5	100_HPS_0
28.09282	−16.631381	0.84	5	8	0.5	5	90_HPS_1.5 10_HPS_0
28.46777	−16.447119	0.84	8	25	0.5	9	100_HPS_0
28.29346	−16.377225	0.82	16	30	0.7	8	100_HPS_0
28.55389	−16.344736	0.82	16	20	0.6	6	95_HPS_0 3_PCA_0 2_L27_0
28.37744	−16.639092	0.82	4	18	0.6	6	100_HPS_0
28.03476	−16.637584	0.82	9	12	0.9	6	100_HPS_0
28.47452	−16.436175	0.82	7	8	0.5	7	100_HPS_0
28.02908	−16.605236	0.82	16	50	0.4	4	70_HPS_38 30_HPS_0
28.12925	−16.529170	0.82	8	9	0.5	5	100_HPS_0
28.15614	−16.635884	0.81	7	15	0.9	7	5_HPS_38 95_HPS_0
28.50974	−16.193821	0.81	12	12	0.7	6	100_HPS_0
28.38366	−16.611910	0.8	12	25	0.8	7	50_HPS_3 50_HPS_0
28.35657	−16.734756	0.8	7	10	0.7	7	100_HPS_3
28.09959	−16.680719	0.8	8	9	0.9	6	10_HPS_0 90_HPS_38
28.38511	−16.584514	0.8	24	10	0.9	9	100_PCA_0
28.37792	−16.570143	0.8	7	18	0.6	6	100_PCA_0
28.45926	−16.420817	0.78	8	12	0.6	9	100_HPS_0
28.35389	−16.373236	0.78	16	10	0.8	5	95_HPS_0 5_MH_0
28.09810	−16.617865	0.78	6	6	0.7	5	90_HPS_38 10_HPS_0
28.37363	−16.652382	0.78	6	10	0.9	5	40_HPS_0 60_HPS_2
28.18275	−16.480165	0.77	8	12	0.7	6	100_HPS_0
28.38805	−16.506205	0.75	10	9	0.9	6	100_HPS_1
28.25800	−16.426538	0.74	8	100	0.05	6	80_HPS_3 20_HPS_20
28.41205	−16.504643	0.74	10	28	0.5	5	60_HPS_0 40_PCA_0
28.36623	−16.499300	0.74	4	15	0.5	8	100_HPS_0
28.40159	−16.509613	0.73	4	18	0.9	5	100_HPS_0
28.38382	−16.596720	0.73	8	9	0.5	4	100_HPS_0
28.15916	−16.766020	0.73	10	7	0.6	6	97_HPS_0 3_HPS_1
28.08029	−16.680308	0.7	14	10	0.7	6	100_HPS_0
28.33809	−16.419592	0.7	7	7	0.9	5	95_HPS_0 5_HPS_38
28.04859	−16.660106	0.69	8	16	0.7	6	100_HPS_0
28.33082	−16.399790	0.69	6	8	0.9	5	100_HPS_0
28.26909	−16.819540	0.69	10	18	0.5	7	97_PCA_0 3_L27_0
28.10252	−16.587477	0.65	8	10	0.7	6	100_HPS_0
28.01262	−16.668922	0.65	12	8	0.9	8	75_HPS_0 25_HPS_3
28.07459	−16.694939	0.64	6	12	0.6	4	90_HPS_1.5 10_HPS_0
28.15323	−16.728272	0.63	6	12	0.75	6	100_HPS_0
28.28033	−16.409189	0.62	8	9	0.5	6	100_HPS_0
28.11100	−16.595715	0.62	10	20	0.7	7	40_HPS_38 10_HPS_1.5 50_HPS_3

Table A1 – *continued*

Latitude (deg)	Longitude (deg)	Radius (km)	Obst. height (m)	Obst. distance (m)	Obst. filling factor –	Lamp height (m)	Lamp spectra and ULOR
28.37534	−16.584072	0.62	9	7	0.6	8	100_PCA_0
28.37693	−16.512386	0.61	8	13	0.7	8	100_HPS_0
28.34693	−16.722251	0.61	6	20	0.7	6	100_HPS_1
28.32740	−16.804861	0.61	8	4	0.5	7	97_PCA_0 3_L27_0
28.23876	−16.796690	0.6	8	14	0.75	8	100_HPS_3
28.39785	−16.554391	0.6	8	15	0.7	7	100_HPS_3
28.44270	−16.282202	0.6	7	30	0.95	7	90_HPS_0 10_MH_5
28.39578	−16.544884	0.59	10	65	0.6	9	80_HPS_0 20_MH_15
28.29615	−16.815608	0.59	8	27	0.4	7	97_PCA_0 3_L27_0
28.43321	−16.321034	0.59	8	17	0.8	6	100_HPS_0
28.18253	−16.818130	0.58	14	10	0.8	6	95_HPS_0 5_L27_0
28.51595	−16.360996	0.58	8	40	0.1	4	100_HPS_0
28.39829	−16.357672	0.57	4	10	0.3	6	100_HPS_1
28.42350	−16.318772	0.57	12	17	0.6	7	95_HPS_2 2.5_MH_2 2.5_FLU_2
28.16574	−16.430795	0.57	6	22	0.7	6	50_HPS_0 50_HPS_50
28.04286	−16.614751	0.56	6	25	0.8	6	80_MH_50 20_HPS_0
28.42400	−16.299263	0.56	15	15	0.8	7	80_HPS_0 20_L40_10
28.05432	−16.525011	0.55	8	25	0.8	4	100_HPS_0
28.40166	−16.321832	0.54	5	7	0.7	7	95_HPS_0 5_MH_5
28.41454	−16.317553	0.54	6	17	0.5	10	100_HPS_3
28.37970	−16.360827	0.53	30	20	0.6	10	95_HPS_0 5_MH_0
28.23671	−16.440496	0.53	16	20	0.6	6	100_HPS_0
28.43874	−16.369566	0.53	7	25	0.4	9	100_HPS_0
28.42918	−16.307490	0.52	7	13	0.9	7	95_HPS_0 5_MH_0
28.49136	−16.214020	0.52	10	30	0.4	7	80_HPS_0 20_MH_5
28.06746	−16.625952	0.52	5	22	0.8	8	40_HPS_38 10_HPS_1.5 50_HPS_3
28.18666	−16.765573	0.51	12	9	0.5	8	30_HPS_3 70_HPS_0
28.33915	−16.790778	0.51	8	7	0.5	6	50_HPS_1 50_HPS_38
28.38759	−16.561770	0.51	9	15	0.7	8	100_PCA_0
28.32649	−16.787447	0.51	8	12	0.5	6	50_HPS_38 50_HPS_0
28.14390	−16.443432	0.5	6	8	0.9	5	100_HPS_38
28.48085	−16.245588	0.5	30	30	0.6	7	90_HPS_0 10_MH_3
28.23301	−16.456764	0.5	8	10	0.4	6	100_HPS_0
28.06971	−16.510903	0.5	7	100	0.05	9	100_L40_100
28.12227	−16.462628	0.5	9	6	0.9	6	100_HPS_1
28.33926	−16.756488	0.48	8	15	0.1	7	100_HPS_0
28.22711	−16.782947	0.48	4	8	0.8	7	95_HPS_1 5_HPS_0
28.40917	−16.333454	0.48	5	10	0.7	10	100_HPS_0
28.49304	−16.354686	0.47	6	12	0.6	8	95_HPS_0 5_PCA_0
28.39138	−16.670902	0.47	6	15	0.8	6	100_HPS_0
28.56031	−16.218691	0.47	4	7	0.8	6	100_HPS_0
28.40934	−16.311675	0.46	10	15	0.5	9	100_HPS_0
28.26815	−16.806913	0.46	9	7	0.6	7	97_PCA_0 3_L27_0
28.39667	−16.347677	0.46	4	8	0.9	4	75_HPS_1 25_HPS_0
28.34160	−16.731272	0.44	4	6	0.7	7	80_HPS_1 20_HPS_0
28.10510	−16.559746	0.43	4	25	0.4	6	99_HPS_0 1_HPS_38
28.52626	−16.154935	0.43	10	11	0.5	7	100_HPS_0
28.18068	−16.792192	0.41	12	12	0.8	9	100_HPS_0
28.39212	−16.657583	0.41	6	20	0.6	4	100_HPS_0
28.09897	−16.481605	0.41	6	6	0.9	6	100_HPS_1
28.16870	−16.733814	0.4	5	30	0.2	6	99_HPS_0 1_FLU_38
28.39388	−16.591268	0.4	9	15	0.9	5	90_PCA_0 10_HPS_0
28.14233	−16.522501	0.4	8	10	0.5	5	100_HPS_0
28.41704	−16.304883	0.4	5	10	0.8	4	100_HPS_0
28.19417	−16.424306	0.4	9	40	0.3	7	100_HPS_0
28.27356	−16.384774	0.4	8	16	0.75	6	100_HPS_0
28.38185	−16.373466	0.4	10	7	0.7	9	90_HPS_2 10_HPS_0
28.38211	−16.534929	0.4	8	22	0.8	4	100_HPS_0
28.36673	−16.528122	0.38	8	12	0.6	5	100_PCA_0
28.38796	−16.553718	0.37	9	10	0.8	5	100_HPS_0
28.14599	−16.792426	0.37	48	40	0.5	7	100_HPS_2
28.39359	−16.649390	0.37	8	13	0.7	5	100_HPS_0
28.40723	−16.325813	0.36	8	20	0.7	4	100_HPS_0

Table A1 – *continued*

Latitude (deg)	Longitude (deg)	Radius (km)	Obst. height (m)	Obst. distance (m)	Obst. filling factor –	Lamp height (m)	Lamp spectra and ULOR
28.28347	−16.801950	0.36	4	8	0.7	3	97_PCA_0 3_L27_0
28.48806	−16.238554	0.35	12	6	0.8	6	100_HPS_0
28.15812	−16.746611	0.35	7	20	0.2	7	99_HPS_0 1_HPS_1
28.17986	−16.802851	0.34	12	9	0.75	6	100_HPS_0
28.40318	−16.332080	0.33	8	10	0.8	6	95_HPS_15 5_MH_15
28.43660	−16.288420	0.32	7	60	0.2	7	80_HPS_0 20_MH_5
28.22189	−16.413374	0.31	8	12	0.6	7	100_HPS_0
28.29604	−16.565715	0.29	8	45	0.2	4	100_FLU_15
28.57158	−16.197841	0.29	12	4	0.95	6	100_HPS_0
28.28710	−16.813983	0.29	6	9	0.5	7	97_PCA_0 3_L27_0
28.45347	−16.342539	0.29	6	17	0.95	7	100_MH_5
28.39628	−16.641086	0.28	6	8	0.9	6	95_HPS_0 5_PCA_0
28.24050	−16.403156	0.25	12	10	0.9	7	100_HPS_0
28.10965	−16.470852	0.25	7	13	0.7	7	100_HPS_3
28.14601	−16.547024	0.24	4	10	0.6	6	95_HPS_0 5_HPS_3
28.26879	−16.426897	0.24	6	9	0.7	8	100_HPS_0
28.10215	−16.476654	0.23	8	10	0.9	7	100_HPS_2
28.10540	−16.473615	0.21	10	9	0.9	6	100_HPS_1
28.24013	−16.411299	0.21	5	5	0.85	6	100_MH_3
28.24899	−16.398963	0.19	12	4	0.7	7	100_HPS_0
28.26028	−16.392639	0.13	8	10	0.6	5	100_HPS_0
28.30583	−16.564861	0.06	6	100	0.4	6	100_MV3_15

This paper has been typeset from a TEX/LATEX file prepared by the author.